Journal of Power Sources 195 (2010) 1872–1879

Contents lists available at ScienceDirect

Journal of Power Sources

journal homepage: www.elsevier.com/locate/jpowsour

Modeling of molten carbonate fuel cell based on the volume–resistance characteristics and experimental analysis

Aiguo Liu*, Yiwu Weng

The Key Laboratory of Machinery and Power Engineering of Education Ministry, Shanghai Jiao Tong University, Dongchuan Road No. 800, Shanghai 200240, PR China

ARTICLE INFO

Article history:
Received 5 August 2009
Received in revised form 14 October 2009
Accepted 14 October 2009
Available online 23 October 2009

Keywords:
Molten carbonate fuel cell
Volume–resistance characteristic modeling
Distributed-lumped parameter method
Experiment

ABSTRACT

The real-time dynamic simulation of MCFC is still difficult up to now. This work presents a one-dimensional mathematical model for MCFC considering the variation of local gas properties, and the experimental analysis for the validation of model. The volume–resistance (*V–R*) characteristic modeling method has been introduced. Using the *V–R* modeling method and the modular modeling idea, the partial differential equations for cell mass, energy and momentum balance can be modified in order to develop a model for quick simulation. Experiments have been carried out at Shanghai Jiaotong University Fuel Cell Research Institute. The experiments have been done under different operating pressures, and the results are used to validate the model. A good agreement between simulation and experimental results has been observed. Steady- and dynamic-state simulation results are analyzed. The results indicate that the *V–R* characteristic modeling method is feasible and valuable. The model can be used in the real-time dynamic simulation.

1. Introduction

Molten carbonate fuel cell (MCFC) is high-temperature fuel cell, which has the potential for application in centralized or decentralized power plants with resultant higher efficiency and lower emission. MCFC technology is now at the stage of scaling-up to commercialization.

Many theoretical models have ever been developed for the prediction of MCFC performance [1–13]. Usually the fuel cell models require the consideration of gas flow, heat transfer, mass transfer and cell voltage–current relationship. In addition, the thermal and flow parameters which are functions of temperature and gas composition should be considered. Different numerical analysis methods have ever been applied to investigate the performance of fuel cell, such as fluid dynamics, heat transfer theories, computational fluid dynamics and so on. However, the complete solution algorithm is a complicated iteration process which does not meet the requirement of a real-time dynamic simulation. Simplification does help to get faster solution, but the simplification needs to be evaluated whether it can guarantee a reliable computation result [12,13]. So it is necessary to develop a model which can meet the real-time dynamic simulation with reliable results.

A one-dimension distributed parameters MCFC model has been developed in this work considering the local flow properties, heat transfer, chemical and electrochemical phenomena. The volume–resistance characteristics modeling method was introduced into the MCFC system to satisfy the quick dynamic simulation. Experiments were also carried out at Shanghai Jiaotong University Fuel Cell Research Institute. The comparison of Matlab/Simulink distributed parameter model with experiment result was presented to confirm the accuracy of model. Steady- and dynamic-state simulation results were presented and discussed. This model can be used in the design of control system and semi-physical real-time simulation

2. MCFC mathematical model

Fig. 1 presents the schematic principle view of a co-flow planar MCFC cell, the specifications and related parameters of the MCFC are shown in Table 1.

In order to simplify the model, the following assumptions have been made:

(1) The reactant and products are ideal gas mixture.
(2) Only H_2 is electrochemically oxidized and CO is considered in water–gas shift reaction.
(3) Current collector is ideal conductor without voltage gradients.
(4) Adiabatic boundaries.

* Corresponding author. Tel.: +86 13585630117; fax: +86 2134206342.
E-mail address: liuaiguo119@yahoo.com.cn (A. Liu).

0378-7753/$ – see front matter © 2009 Elsevier B.V. All rights reserved.
doi:10.1016/j.jpowsour.2009.10.040

Nomenclature

A	surface or cross-section area (m^2)
C_p	specific heat capacity ($J\,kg^{-1}\,K^{-1}$)
C_i	molar concentration of component i ($mol\,m^{-3}$)
d_h	hydraulic diameter of gas channel (m)
F	Faraday constant (C)
G	mass flow rate ($kg\,s^{-1}$)
h	height of the channel (m)
H	specific enthalpy ($k\,kg^{-1}$)
I	local current density ($A\,m^{-2}$)
k	heat transfer coefficient ($W\,m^{-1}\,K^{-1}$)
L	cell length (m)
M	molecular weight ($kg\,mol^{-1}$)
P	pressure (Pa)
R	gas constant ($J\,mol^{-1}\,K^{-1}$)
u	velocity in gas channels ($m\,s^{-1}$)
V	voltage (V)
W	cell width (m)

Greek letters

ΔH	enthalpy change of reaction ($J\,mol^{-1}$)
ε	emissivity
λ	thermal conductivity ($W\,m^{-1}\,K^{-1}$)
μ	dynamic viscosity ($kg\,m^{-1}\,s^{-1}$)
ν	stoichiometric coefficient
ρ	density ($kg\,m^{-3}$)
σ	Stefan–Boltzmann constant $5.676e-8$ ($W\,m^{-2}\,K^{-4}$)
τ	thickness of solid structure (m)

Subscripts

anod	anode channel
cath	cathode channel
electrolyte	electrolyte
INTC	interconnector
PEN	positive-electrode/electrolyte/negative-electrode

2.1. Balance equations

A set of partial differential equations based on the conservation equations have been established for the distributed parameter MCFC model as shown in Appendix A. The mathematical model consists of two species mass, two total mass and two moment balance equations to the cathode and anode channels, four energy balance equations to the cathode and anode channels, positive-electrode/electrolyte/negative-electrode (PEN) and interconnector.

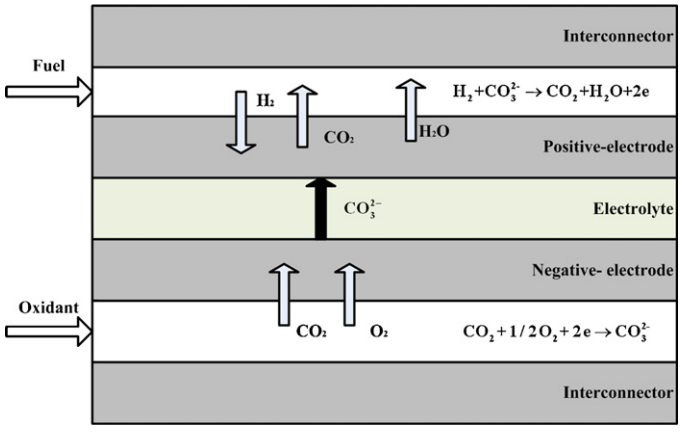

Fig. 1. Schematic principle view of a co-flow planar MCFC.

The species mass balance equations (A.1) and (A.2) are shown in Appendix A. For the anode channel, the chemical elements considered are H_2, CO, CO_2, and H_2O, while for the cathode channel the chemical species are O_2, N_2, and CO_2. The external reforming MCFC technology has been considered, hence, there is no steam reforming reaction in the anode channel. The CO in the anode channel is not involved in the electrochemical reaction but in the water–gas shift reaction. The water gas shift reaction is very fast. The equations concerning water gas shift reaction are shown as follows. And the equilibrium limited shift reaction rate expressions are derived from Aguiar et al. [14,15].

$$\text{Watergasshiftreaction}: \quad CO + H_2O \Leftrightarrow CO_2 + H_2 \tag{1}$$

$$\text{Reaction rate}: \quad R_I = k_{WGSR} p_{anod,CO} \left(1 - \frac{p_{anod,CO_2} p_{anod,H_2}}{k_{shift} p_{anod,CO} p_{anod,H_2O}}\right) \tag{2}$$

$$\text{Equilibrium constant}: \quad k_{shift} = \exp\left(\frac{4276}{T_{anod}} - 3.961\right) \tag{3}$$

(A.3) and (A.4) shown in Appendix A are the total mass balance equations. For the anode channel two reactions are taken into account: water gas shift reaction and hydrogen electrochemical oxidation. In the cathode channel only the reduction reaction of O_2 and CO_2 to CO_3^{2-} ions is considered. The reaction kinetics equations related with electrochemical reaction are given in detail as follows.

$$\text{Anode}: \quad H_2 + CO_3^{2-} \rightarrow CO_2 + H_2O + 2e^- \tag{4}$$

$$\text{Cathode}: \quad CO_2 + \frac{1}{2}O_2 + 2e^- \rightarrow CO_3^{2-} \tag{5}$$

$$\text{Reaction rate}: \quad R_{(II,III)} = \frac{I}{2F} \tag{6}$$

Momentum balance equations (A.5) and (A.6) are also added to indicate the pressure distribution in the gas channels. The $f(W,h)$ in momentum balance equations is the function of geometry parameters W and h of MCFC [14].

Four energy balance equations (A.7)–(A.10) in Appendix A are considered for accurately calculation the temperature profile in the relevant part of cell. Different heat transfer modes have been considered for different parts of the MCFC. The thermal flux of the interconnector and the PEN includes thermal conduction, thermal convection and thermal radiation. In addition, the enthalpy flux associated with the flow of oxygen, carbon dioxide and hydrogen to the PEN structure and water and carbon dioxide from the PEN structure has also been taken into account. The thermal flux in the gas channel is convective from the solid parts and the enthalpy flux associated with the species flow between PEN and gas channel. The detailed balance equations are referred to Refs. [14–16].

Detailed gas thermal and transport properties such as density, specific heat capacity, thermal conductivity and dynamic viscosity are considered for the accuracy of model. The pure gas properties are all functions of temperature, whereas the properties of gas mixtures can be estimated as a function of pure gas properties and gas composition [17–19]. Concerning the solid phase of the PEN and the interconnector, the thermal conductivity and the specific heat are needed in the energy balance equations. The interconnector is made of stainless steel for which its property data are well known. While the PEN structure is composed of Ni-alloy anode, Ni oxide cathode, molten carbonate electrolyte and porous ceramic matrix, which is difficult to estimate its thermal conductivity and

Table 1
Specification of the MCFC model and parameters.

Variable	Specification
Cell length, L	0.4 m
Cell width, W	0.8 m
Interconnector thickness, τ_{INTC}	0.0008 m
PEN thickness, τ_{PEN}	0.001 m
Gas channel depth, h	0.0008 m
PEN density, ρ_{PEN}	2000 kg m^{-3}
PEN specific heat, $C_{p,PEN}$	800 J kg^{-1} K^{-1}
PEN thermal conductivity, λ_{PEN}	16.2 W m^{-1} K^{-1}
Interconnector density, ρ_{INTC}	8100 kg m^{-3}
Interconnector specific heat, $C_{p,INTC}$	462 J kg^{-1} K^{-1}
Interconnector thermal conductivity, λ_{INTC}	22 W m^{-1} K^{-1}
Emissivity from interconnector, ε_{INTC}	0.286
Emissivity from PEN, ε_{PEN}	0.118
Inlet fuel temperature, $T_{anod,1}$	853 K
Inlet oxidant temperature, $T_{cath,1}$	843 K
Inlet fuel and oxidant pressure, $P_{anod,1}$ $P_{cath,1}$	1.1×10^5 Pa
Inlet fuel mass flow rate, G_{anod}	5.2×10^{-5} kg s^{-1}
Inlet oxidant mass flow rate, G_{cath}	1.775×10^{-3} kg s^{-1}
Fuel composition	H_2 60%, CO_2 10%, CO 20%, H_2O 10%
Oxidant composition	CO_2 30%, air 70%,
Parameters in electrochemical model	$C_1 = 3.28 \times 10^{-9}$; $C_2 = 3.39 \times 10^{-6}$; $C_a = 2.04 \times 10^{-3}$; $C_{ir} = 1.12 \times 10^{-2}$; $\Delta H_{C_1} = 132,000$; $\Delta H_{C_2} = 67,100$; $\Delta H_a = 23,700$; $\Delta H_{ir} = 23,000$

specific heat. Therefore a constant value has been given based on the literature [19].

2.2. Electrochemical model

The electrochemical model that relates the gas compositions and temperatures to voltage, current density and other cell variables has been developed. In ideal case the change in Gibbs free energy is available as useful electric energy at the temperature of conversion. The Gibbs free energy change can be expressed as a function of temperature, and the maximum reversible potential of the MCFC is connected with the Gibbs free energy change [20]. But the actual operating potential will decrease from its maximum reversible potential because of the irreversible losses. Several sources contribute to irreversible losses in a practical fuel cell. The losses, which are often called polarization, originate from three sources: activation polarization, ohmic polarization and concentration polarization. The electrochemical model has been shown as Eqs. (7)–(12) [21,22]:

$$\text{Nernst potential}: \quad E = E_0 + \frac{RT}{2F}\ln\left[\frac{P_{H_2,anod}(P_{O_2,cath})^{1/2}P_{CO_2,cath}}{P_{H_2O,anod}P_{CO_2,anod}}\right] \tag{7}$$

$$\text{Current density}: \quad I = \frac{E - V}{R_{tol}} \tag{8}$$

$$\text{Total irreversible loss}: \quad R_{tol} = R_{anod} + R_{cath} + R_{ir} \tag{9}$$

$$\text{Anode irreversible loss}: \quad R_{anod} = C_a e^{\Delta H_a/RT} P_{H_2,anod}^{-0.5} \tag{10}$$

$$\text{Cathode irreversible loss}: \quad R_{cath} = (C_1 e^{\Delta H_{C_1}/RT} P_{O_2,cath}^{-0.75} P_{CO_2,cath}^{0.5}) + (C_2 e^{\Delta H_{C_2}/RT} M_{CO_2,cath}^{-1}) \tag{11}$$

$$\text{Internal cell resistance}: \quad R_{ir} = C_{ir} e^{\Delta H_{ir}/RT} \tag{12}$$

where E_0 is the ideal standard potential for the cell reaction and the parameters C and ΔH are related to electrodes and electrolyte which can be found in Ref. [21]. $LiNaCO_3$ is considered as electrolyte in this modeling.

2.3. Solution strategy

The dynamic balance equations for a distributed parameter MCFC model have been shown above. It includes nonlinear partial differential equations which makes it difficult to solve. More importantly, the coupling of pressure and flow rate will cause the iteration solution. In the conventional iteration algorithm, the calculation is very time consuming and the convergence time cannot be determined owing to the short time step and the uncertainty of iteration times. The *V–R* modeling method has ever been developed and used for heat exchanger and solid oxide fuel cell [16,23]. The key point of the *V–R* model is noniterative algorithm in the calculation. The time consuming is shorter compared with the finite difference model and finite volume model, which can guarantee the real-time characteristics of the model. Here the *V–R* modeling method will be introduced into the MCFC system.

2.3.1. V–R characteristic modeling method

In the fluid system, each component can be treated as one of three types: volume module, resistance module and volume–resistance module. The volume module is the component which can neglect the pressure loss and accumulate fluid based on the difference of flow rates between the inlet and outlet. The pressure can be considered as constant and the mass flow rate is the state variable in the component. Whereas in the resistance module, the fluid has an obvious pressure loss, and the flow rate of the component can be determined by the pressure difference. So the mass flow rate can be considered as constant and the pressure is the state variable. MCFC is such a kind of component which has the quality of both the volume module and resistance module.

In general, the volume module can be described as follows:

$$\frac{dP}{dt} = \frac{RT}{dx}(G_1 - G_2) \tag{13}$$

The resistance model can be described as:

$$\frac{dG}{dt} = \frac{A(P_1 - P_2)}{dx} - \frac{2fG^2}{A\rho d_h} \tag{14}$$

The *V–R* modeling method is based on the lumped parameter idea. In order to depict the distributed parameter model, the MCFC component will be divided into several control units as shown in Fig. 2. The grid meshing along the flowing direction can be applied to co-flow and counter-flow MCFC. When applying the model to

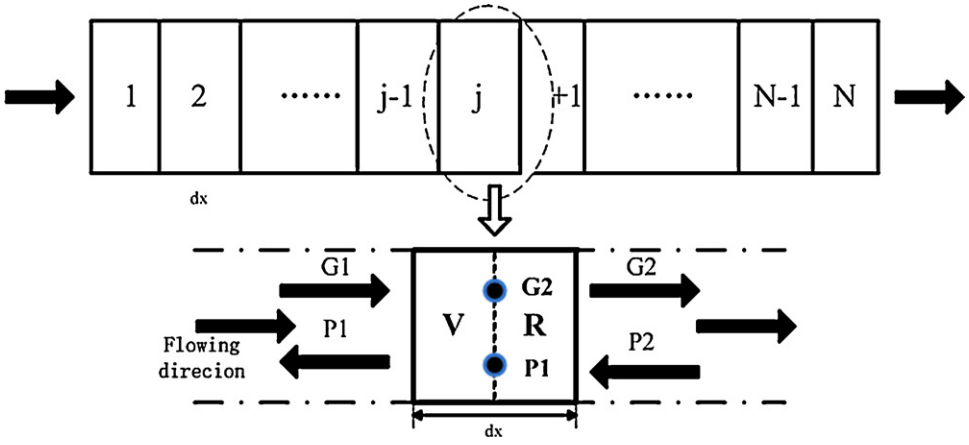

Fig. 2. Diagram of grid mark for flow rate and pressure.

counter-flow MCFC, the grid will be numbered along individual flow directions of the hot fluid and the cold fluid, respectively. All flow and thermal properties are uniform at the same unit. In each control unit, the module will be separated into two sub-modules: volume module and resistance module. In the volume module, the pressure is considered constant and the mass flow rate is the state variable. In the resistance module, the mass flow rate is considered constant and the pressure is the state variable. Thus it is not necessary to assume pressure or flow rate as constant to solve the mathematic model through iteration algorithm. The pressure and flow rate will be decoupled through two state variables in individual modules.

2.3.2. MCFC V–R characteristics model

Based on the idea above, one set of equations for the fluid in the control section can be obtained. The partial differential equations can be converted to ordinary differential equations.

Using the mass and momentum conservation principle the following equations can be obtained from the volume and resistance module:

$$\frac{dP}{dt} = \frac{RT_i}{M}\left[-\frac{G_i - G_{i+1}}{Adx} - (\nu_{O_2,III}M_{O_2} + \nu_{CO_2,III}M_{CO_2})\frac{R_{III}}{h}\right] \tag{15}$$

$$\frac{dG}{dt} = -A\frac{P_{i+1} - P_i}{dx} - 2f(W,h)\frac{\mu uA}{d_h^2} \tag{16}$$

The species mass and energy balance equations can be merged into one control section. Based on the above idea, one set of equations can be obtained as shown in Table 2.

2.3.3. MCFC model solution

The geometrical parameters of the fuel cell and some other thermodynamic and electrical properties have been given in Table 1. All the static variables such as molar components, flow rate and temperatures were given an initial value. The boundary condition, i.e.

Table 2
MCFC balance equations.

Anode channel:

$$\frac{dC_{anod,i}}{dt} = -\frac{C_{anod,i,2}u_{anod,2} - C_{anod,i,1}u_{anod,1}}{\partial x} + \sum_{k=(I,II)}\nu_{i,k}R_{k,2}\frac{1}{h_{anod}},\ i = (H_2, CO, CO_2, H_2O)$$

$$\frac{dG_{anod,2}}{dt} = -A_{anod}\frac{P_{anod,2} - P_{anod,1}}{dx} - 2f(W,h_{anod})\frac{\mu_{anod,2}u_{anod,2}A_{anod}}{d_{h,anod}^2}$$

$$\frac{dP_{anod,2}}{dt} = \frac{RT_{anod,2}}{M_{anod,2}}\left[-\frac{G_{anod,2} - G_{anod,1}}{A_{anod}dx} - (\nu_{O_2,III}M_{O_2} + \nu_{CO_2,III}M_{CO_2})\frac{R_{III}}{h_{anod}}\right]$$

$$\frac{dT_{anod}}{dt} = -\frac{u_{anod,2}T_{anod,2} - u_{anod,1}T_{anod,1}}{dx} + \frac{1}{\rho_{anod,2}C_{p,anod,2}h_{anod}}\left[\sum_{i=H_2,H_2O,CO_2}\nu_{i,III}R_{III}h_i + k_{anod,PEN,2}(T_{PEN,2} - T_{anod,2}) + k_{anod,INTC,2}(T_{INTC,2} - T_{anod,2}) + (-\Delta H)_{I,2}R_{I,2}\right]$$

Cathode channel

$$\frac{dC_{cath,i}}{dt} = -\frac{C_{cath,i,2}u_{cath,2} - C_{cath,i,1}u_{cath,1}}{dx} + \nu_{i,(III)}R_{(III)}\frac{1}{h_{cath}}\ i = (N_2, CO_2, O_2)$$

$$\frac{dG_{cath,2}}{dt} = -A_{cath}\frac{P_{cath,2} - P_{cath,1}}{dx} - 2f(W,h_{cath})\frac{\mu_{cath,2}u_{cath,2}A_{cath}}{d_{h,cath}^2}$$

$$\frac{dP_{cath,2}}{dt} = \frac{RT_{cath,2}}{M_{cath,2}}\left[-\frac{C_{cath,2} - G_{cath,1}}{A_{cath}dx} + (\nu_{O_2,III}M_{O_2} + \nu_{CO_2,III}M_{CO_2})\frac{R_{III}}{h_{cath}}\right]$$

$$\frac{dT_{cath}}{dt} = -\frac{u_{cath,2}T_{cath,2} - u_{cath,1}T_{cath,1}}{dx} + \frac{1}{\rho_{cath,2}C_{p,cath,2}h_{cath}}\left[\sum_{i=O_2,CO_2}\nu_{i,III}R_{III}h_i + k_{cath,PEN,2}(T_{PEN,2} - T_{cath,2}) + k_{cath,INTC,2}(T_{INTC,2} - T_{cath,2})\right]$$

PEN structure

$$\frac{dT_{PEN,2}}{dt} = \frac{\lambda_{PEN}}{\rho_{PEN}C_{P,PEN}} \times \frac{T_{PEN,3} - 2T_{PEN,2} + T_{PEN,1}}{(dx)^2} -$$

$$\frac{1}{\rho_{PEN}C_{P,PEN}\tau_{PEN}}\left\{k_{anod,PEN,2}(T_{PEN,2} - T_{anod,2}) + k_{cath,PEN,2}(T_{PEN,2} - T_{cath,2}) + \sum_{i=H_2,H_2O,CO_2}\nu_{i,(III)}R_{(III)}h_i + \sum_{i=O_2,CO_2}\nu_{i,(III)}R_{III}h_i + IU - \left[\frac{\sigma(T_{INTC,2}^4 - T_{PEN,2}^4)}{(1/\varepsilon_{INTC}) + (1/\varepsilon_{PEN}) - 1}\right]\right\}$$

Interconnector:

$$\frac{dT_{INTC,2}}{dt} = \frac{\lambda_{INTC}}{\rho_{INTC}C_{P,INTC}} \times \frac{T_{INTC,3} - 2T_{INTC,2} + T_{INTC,1}}{(dx)^2} - \frac{1}{\rho_{INTC}C_{P,INTC}\tau_{INTC}}\left\{k_{anod,INTC,2}(T_{INTC,2} - T_{anod,2}) + k_{cath,INTC,2}(T_{INTC,2} - T_{cath,2}) + \left[\frac{\sigma(T_{INTC}^4 - T_{PEN}^4)}{(1/\varepsilon_{INTC}) + (1/\varepsilon_{PEN}) - 1}\right]\right\}$$

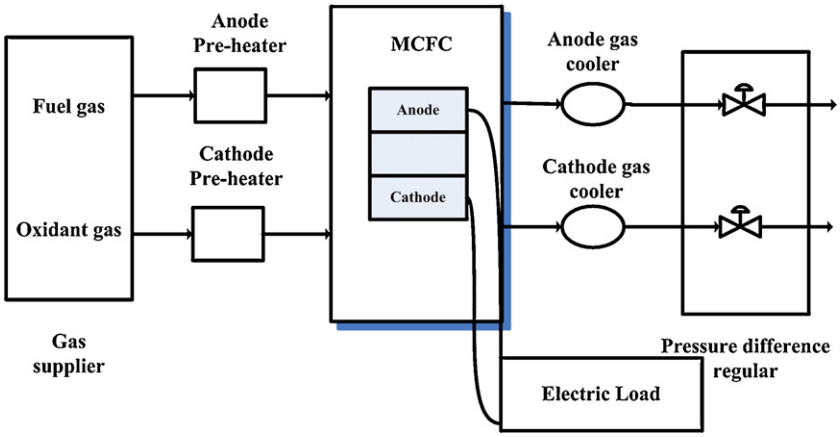

Fig. 3. MCFC power system schedule.

the thermal flux density of both the inlet and the outlet for the solid parts were considered to be zero.

The partial differential equations for MCFC have been converged to the ordinary differential equations based on the *V–R* characteristic modeling. And then the cell length is divided into 20 sub-divisions along the flow direction as shown in Fig. 2 ($N = 20$). The *V–R* characteristic modeling is used in each sub-division. The one-dimension distributed parameters modeling of MCFC can be realized combined with this distributed-lumped parameter method. In many simulation platforms there are perfect algorithms for the solution of ordinary differential equation. Here the system model is developed and solved on the Matlab/Simulink simulation platform with the boundary and initial conditions in Table 1.

3. Experimental analysis

Some experimental tests have been conducted on a parallel plate MCFC. The fuel cell temperature was measured through thermocouple inserted in inlet, exit and the middle of cathode channel. A complete characterization of the cell electrical behavior has been obtained through voltage–current measures under different operating pressure. The experimental results would be used to perform a calibration of the model.

3.1. Test facility

The fuel cell power system scheme is shown in Fig. 3. The test system consists of pre-heater, control valve, cooler, pressure regulator and a software which controls the sub-units and performs the test data acquisition.

The fuel and oxidant are supplied by the gas supplier in which the pre-mixed gas is formed. The molar compositions of fuel are H_2 60%, CO_2 10%, CO 20%, H_2O 10% and the mass flow rate is 0.052×10^{-3} kg s^{-1}. The oxidant molar compositions are CO_2 30%, air 70% with the mass flow rate 1.775×10^{-3} kg s^{-1}. The gas flow is controlled by two thermal mass flow regulators. The anode and cathode pre-heater can heat the fuel and oxidant to the needed temperature. The pressure regulator can regulate the fuel cell operating pressure. The power generated by the stack is fed to the power circuit made by the series of the electronic load.

3.2. Test results

The test period lasted for nearly 500 h. A series of tests have been performed. The test aimed at determining the electrical behavior of fuel cell by changing the operating pressure. The test results would be compared with the simulation results to confirm the accuracy of modeling. The fuel cell temperature was kept constant using heating plates. The related experimental characteristic curve obtained at three different pressures has been shown in Fig. 4.

4. Result and discussion

4.1. Model validation

A model validation has been performed utilizing data from experiment. Validation allows finding the accuracy of the model.

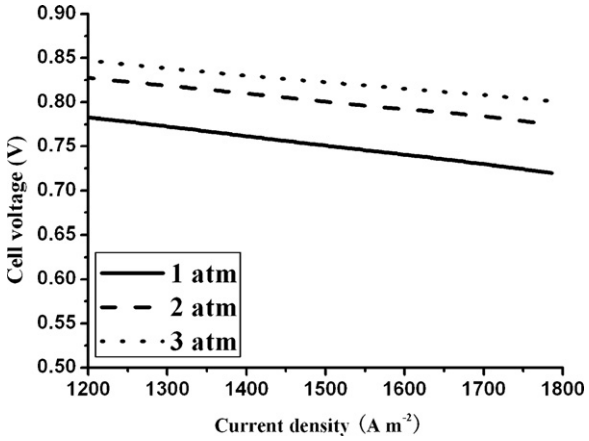

Fig. 4. Measured characteristic curves at different pressures.

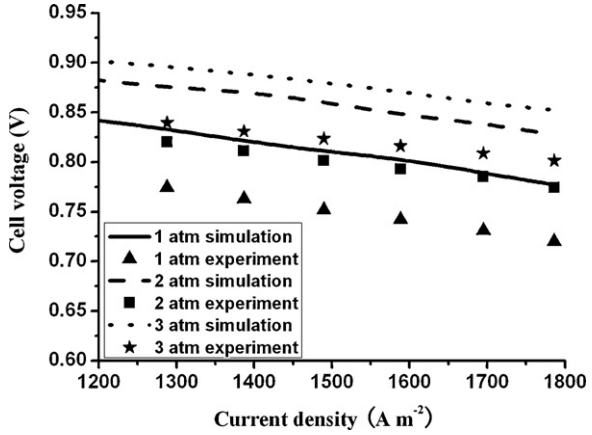

Fig. 5. Experimental and calculated values comparison.

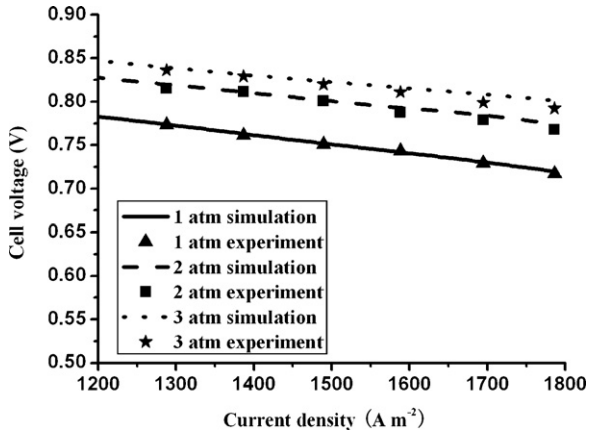

Fig. 6. Experimental and calculated values comparison after revision.

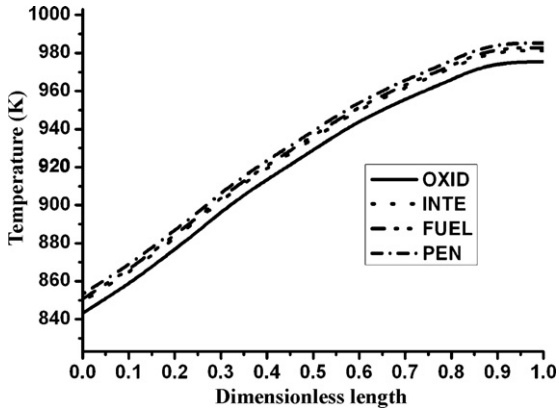

Fig. 7. Temperature profile along the cell length.

Comparisons of polarization curves under different operating conditions are shown in Fig. 5. The difference between model prediction and experiment result is large for cell voltage. The maximum deviation is nearly 10%, and the model prediction is always higher than experimental result. This situation can be explained as the existence of parasitic currents between electrodes depending on specific cell manufacturing features, which are difficult to be evaluated [24,25]. So the calculated voltage can be corrected with an offset parameter 0.06 V. With the additional assumption the average absolute difference between model and experiment results is limited to 1%. The comparison was shown in Fig. 6 after being corrected. The accordance between the model and the experiment confirms the accuracy of model.

4.2. Simulation results

4.2.1. Steady-state results

The performances of MCFC were calculated at atmospheric pressure and 923 K. Calculated temperature profiles of the fuel channel, oxidant channel, interconnector and PEN structure along the cell length were presented in Fig. 7. The temperature increased along the gas flow direction owing to the heat accumulation released by the electrochemical and shift reactions. The maximum temperature occurred at the fuel cell exit. Measured temperatures in experiment were the inlet, middle and the exit of cathode channel. The difference between measured values and calculated was less than 10 K.

Fig. 8 presented the profiles of the dimensionless gas properties (pressure, velocity, density, specific heat capacity and dynamic viscosity) along the cell length in the gas channels. The dimensionless gas properties are defined as the ratio of the local values and the corresponding inlet gas properties values. The inlet gas properties can be calculated from the inlet conditions using the methods given in Refs. [18,19]. The results showed that the change of gas properties along the cell length was considerable. Therefore the assumption as a constant value would cause deviation for computation result.

The simulation results above are consistent with Refs. [1,3,4,16], which verifies that the model established is useful and feasible. For the rated case, the predicted values are as follows: the operating voltage is 0.75 V; the average current density is 1500 A m^{-2}; the fuel cell electrical efficiency is 45%.

4.2.2. Dynamic-state results

The dynamic behavior of the fuel cell was investigated based on the basic steady-state case. A 2% step decrease in the fuel molar rate was imposed on the fuel channel when the fuel cell system has operated for 400 s. The fuel utilization is an important parameter which can determine the stable operation of system. So the fuel utilization was kept constant as 0.8 by adopting the PID control technique to adjust the operating voltage.

The responses of the operating voltage and the average current density of the fuel cell were shown in Figs. 9 and 10. When the fuel flow rate was decreased, the predicted average current density dropped to 1470 A m^{-2}, whereas the operating voltage increased to 0.76 V. The dynamic response of the temperature at the exit of

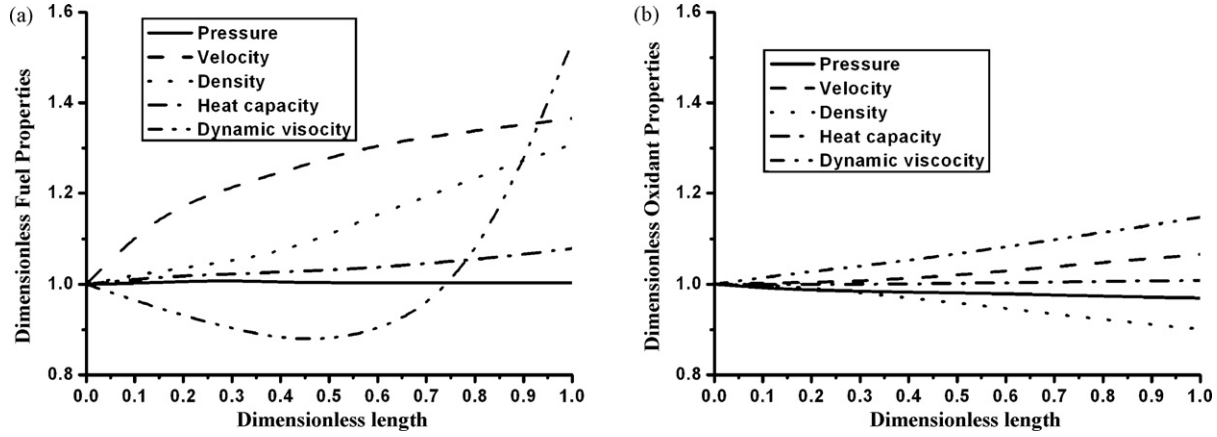

Fig. 8. Gas channel dimensionless property profiles along the cell length.

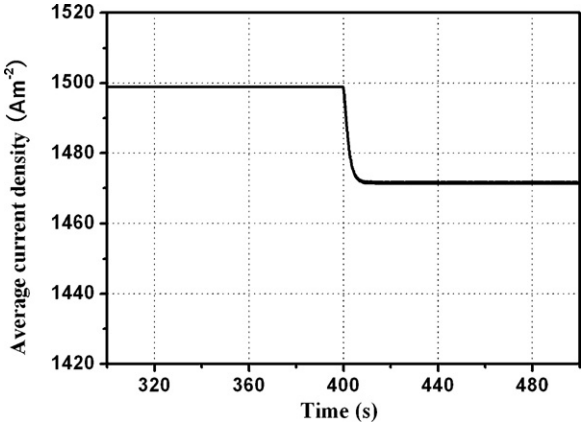

Fig. 9. Dynamic response of average current density.

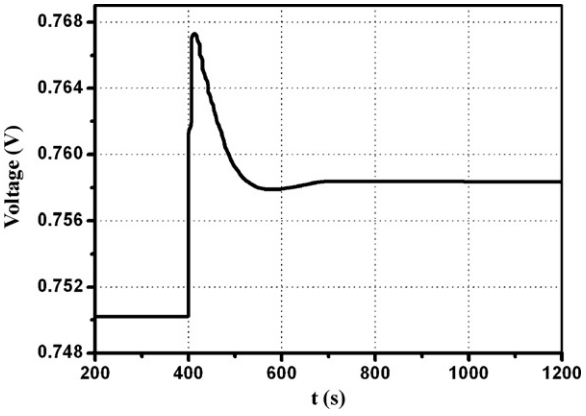

Fig. 10. Dynamic response of operating voltage.

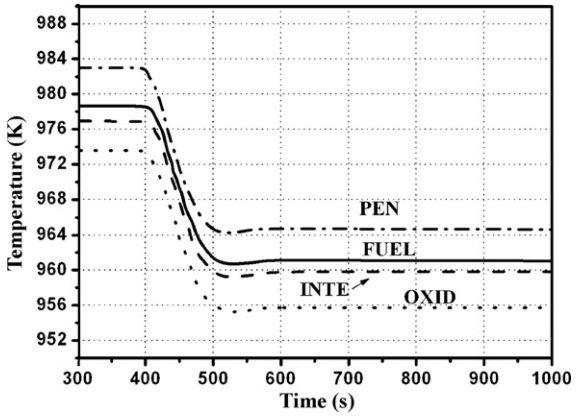

Fig. 11. Temperature dynamic response.

fuel cell was presented in Fig. 11. The time consuming for the solution is nearly 300 s. Using the same computer to calculate the same change with MCFC model in [26,27], the time consuming is 2000 s. The shorter time consuming can meet the real-time simulation requirement.

According to Figs. 9–11, the inertia delay time of temperature and operating voltage is significantly larger than the current density. The larger inertia delay time of temperature and operating voltage is mainly because of the great thermal capacity of the fuel cell. This result can be useful and meaningful for the design of the control system.

5. Conclusions

A mathematical model of MCFC has been developed using the volume–resistance characteristic modeling method. In addition, experimental results of testing the MCFC under different operating pressures have been presented.

Based on the *V–R* modeling method, the distributed-lumped parameter method and the modular modeling idea, the distributed parameter simulation model was established. This noniterative model can satisfy the requirement of a quick dynamic and real-time simulation. The model has been validated using the results of experiments by developing polarization curve under different operating pressure. The good correlation between simulated and experimental results demonstrates the capacity of the model to predict the cell behavior.

Acknowledgements

This project was supported by National Natural Science Foundation of China (NSFC) under the contract no. 90610019 and the National 863 Plan under the contact no.2007AA05Z134 . The authors thank Lijin Wang for his helpful discussion and FanYang for her help in carrying out experiment.

Appendix A.

Balance equations

Species mass balance equations:

$$\text{Anode channel}: \quad \frac{\partial C_{\text{anod},i}}{\partial t} = -\frac{\partial C_{\text{anod},i} u_{\text{anod}}}{\partial x} + \sum_{k=(\text{I},\text{II})} \nu_{i,k} R_k \frac{1}{h_{\text{anod}}}, \quad i = (\text{H}_2, \text{CO}, \text{CO}_2, \text{H}_2\text{O}) \tag{A.1}$$

$$\text{Cathode channel}: \quad \frac{\partial C_{\text{cath},i}}{\partial t} = -\frac{\partial C_{\text{cath},i} u_{\text{cath}}}{\partial x} + \nu_{i,(\text{III})} R_{(\text{III})} \frac{1}{h_{\text{cath}}}, \quad i = (\text{N}_2, \text{CO}_2, \text{O}_2) \tag{A.2}$$

Mass balance equations:

$$\text{Anode channel}: \quad \frac{\partial \rho_{\text{anod}}}{\partial t} = -\frac{\partial \rho_{\text{anod}} u_{\text{anod}}}{\partial x} - \nu_{\text{O}_2,\text{CO}_2} R_{\text{O}_2,\text{CO}_2} M_{\text{O}_2,\text{CO}_2} \frac{1}{h_{\text{anod}}} \tag{A.3}$$

$$\text{Cathode channel}: \quad \frac{\partial \rho_{\text{cath}}}{\partial t} = -\frac{\partial \rho_{\text{cath}} u_{\text{cath}}}{\partial x} + \nu_{\text{O}_2,\text{CO}_2} R_{\text{O}_2,\text{CO}_2} M_{\text{O}_2,\text{CO}_2} \frac{1}{h_{\text{cath}}} \tag{A.4}$$

Momentum balance equations:

$$\text{Anode channel}: \quad \frac{\partial \rho_{\text{anod}} u_{\text{anod}}}{\partial t} = -\frac{\partial \rho_{\text{anod}} u_{\text{anod}} u_{\text{anod}}}{\partial x} - \frac{\partial P_{\text{anod}}}{\partial x} - \frac{2f(W, h_{\text{anod}}) u_{\text{anod}} \mu_{\text{anod}}}{{d_h}^2} \tag{A.5}$$

$$\text{Cathode channel}: \quad \frac{\partial \rho_{\text{cath}} u_{\text{cath}}}{\partial t} = -\frac{\partial \rho_{\text{cath}} u_{\text{cath}} u_{\text{cath}}}{\partial x} - \frac{\partial P_{\text{cath}}}{\partial x} - \frac{2f(W, h_{\text{cath}}) u_{\text{cath}} \mu_{\text{cath}}}{{d_h}^2} \tag{A.6}$$

Energy balance equations:

$$\text{Anode channel}: \quad \frac{\partial \rho_{\text{anod}} e_{\text{anod}}}{\partial t} = -\frac{\partial (\rho_{\text{anod}} u_{\text{anod}} C_{p,\text{anod}} T_{\text{anod}})}{\partial x} + \left[\sum_{i=\text{H}_2,\text{H}_2\text{O},\text{CO}_2} \nu_{i,\text{III}} R_{\text{III}} h_i + k_{\text{anod,PEN}} (T_{\text{PEN}} - T_{\text{anod}}) + k_{\text{anod,INTC}} (T_{\text{INTC}} - T_{\text{anod}}) + (-\Delta H)_{\text{I}} R_{\text{I}} \right] \frac{1}{h_{\text{anod}}} \tag{A.7}$$

Cathode channel :

$$\frac{\partial \rho_{\text{cath}} e_{\text{cath}}}{\partial t} = -\frac{\partial(\rho_{\text{cath}} u_{\text{cath}} C_{p,\text{cath}} T_{\text{cath}})}{\partial x} + \left[\sum_{i=O_2,CO_2} \nu_{i,\text{III}} R_{\text{III}} h_i + k_{\text{cath,PEN}}(T_{\text{PEN}} - T_{\text{cath}}) + k_{\text{cath,INTC}}(T_{\text{INTC}} - T_{\text{caht}}) \right] \frac{1}{h_{\text{cath}}} \quad \text{(A.8)}$$

PEN structure :

$$\frac{\partial T_{\text{PEN}}}{\partial t} = \frac{\lambda_{\text{PEN}}}{\rho_{\text{PEN}} C_{P,\text{PEN}}} \times \frac{\partial^2 T_{\text{PEN}}}{\partial x^2} - \frac{1}{\rho_{\text{PEN}} C_{P,\text{PEN}} \tau_{\text{PEN}}} \times \left\{ k_{\text{anod,PEN}}(T_{\text{PEN}} - T_{\text{anod}}) + k_{\text{cath,PEN}}(T_{\text{PEN}} - T_{\text{cath}}) + \sum_{i=H_2,H_2O,CO_2} \nu_{i,(\text{III})} R_{(\text{III})} h_i + \sum_{i=O_2,CO_2} \nu_{i,(\text{III})} R_{(\text{III})} h_i + \text{IU} - \left[\frac{\sigma(T_{\text{INTC}}^4 - T_{\text{PEN}}^4)}{(1/\varepsilon_{\text{INTC}}) + (1/\varepsilon_{\text{PEN}}) - 1} \right] \right\} \quad \text{(A.9)}$$

Inter connector :

$$\frac{\partial T_{\text{INTC}}}{\partial t} = \frac{\lambda_{\text{INTC}}}{\rho_{\text{INTC}} C_{P,\text{INTC}}} \times \frac{\partial^2 T_{\text{INTC}}}{\partial x^2} - \frac{1}{\rho_{\text{INTC}} C_{P,\text{INTC}} \tau_{\text{INTC}}} \times \left\{ k_{\text{anod,INTC}}(T_{\text{INTC}} - T_{\text{anod}}) + k_{\text{cath,INTC}}(T_{\text{INTC}} - T_{\text{cath}}) + \left[\frac{\sigma(T_{\text{INTC}}^4 - T_{\text{PEN}}^4)}{(1/\varepsilon_{\text{INTC}}) + (1/\varepsilon_{\text{PEN}}) - 1} \right] \right\} \quad \text{(A.10)}$$

References

[1] H.L. Hao, H.S. Zhang, S.L. Weng, J. Power Sources 161 (2006) 849–855.
[2] Q.-m. Chen, Y.-w. Weng, W. Gu, Power Eng. 25 (2005) 603–608.
[3] F. Yoshiba, T. Abeb, T. Watanabe, J. Power Sources 87 (2000) 21–27.
[4] J.H. Koh, B.S. Kang, H.C. Lim, J. Power Sources 91 (2000) 161–171.
[5] N. Kobayashi, H. Fujimura, K. Ohtsuka, JSME Int. J. 32 (1989) 420–427.
[6] H. Fujimura, N. Kobayashi, K. Ohtsuka, JSME Int. J. 35 (1992) 82–89.
[7] W. He, Q. Chen, J. Power Sources 55 (1995) 25–32.
[8] F. Yoshiba, N. Ono, Y. Izaki, T. Watanabe, T. Abe, J. Power Sources 71 (1998) 328–336.
[9] W. He, Q. Chen, J. Power Sources 73 (1998) 182–192.
[10] Y.R. Lee, I.G. Kim, G.Y. Chung, C.G. Lee, H.C. Lim, T.H. Lim, S.W. Nam, S.A. Hong, J. Power Sources 137 (1998) 9–16.
[11] B. Marcenerro, F. Federici, Proceedings of the International Hydrogen Energy Congress and Exhibition, 2005, pap. FCD244.
[12] F. Standeart, K. Hemmes, N. Woudstra, J. Power Sources 63 (1996) 221–234.
[13] M. Baranak, H. Atakul, T. Sener, F. Akgun, M. Tırıs, Proceedings of the International Hydrogen Energy Congress and Exhibition, Istanbul, Turkey, 23-15, 2005, pap. FCD272.
[14] P. Aguiar, C.S. Adjiman, N.P. Brandon, J. Power Sources 138 (2004) 120–136.
[15] L.J. Wang, H.S. Zhang, S.L. Weng, J. Power Sources 177 (2008) 579–589.
[16] P. Iora, P. Aguiar, C.S. Adjiman, Chem. Eng. Sci. 60 (2005) 2963–2975.
[17] B.E. Poling, J.M. Prausnnitz, J.P. O'Connell, The Properties of Liquids & Gases, 5th ed., McGraw-Hill, New York, 2000.
[18] B. Todd, J.B. Young, J. Power sources 110 (2002) 186–200.
[19] J.H. Koh, H.K. Seo, Y.S. Yoo, Chem. Eng. J. 87 (2002) 367–379.
[20] C. Hitchings, Fuel Cell Handbook, 6th ed., EG&G Technical Services, Inc., Virginia, 2002.
[21] M. Baranak, H. Atakul, J. Power Sources 172 (2007) 831–839.
[22] K. Kordesch, G. Simader, Fuel Cells and Their Applications, VCH, New York, 1996, p. 111.
[23] H. Zhang, S. Weng, M. Su, Proceedings of the ASME TURBO EXPO, USA, 68293, 2005.
[24] E. Arato, B. Bosio, P. Costa, J. Power Sources 102 (2001) 74–81.
[25] S. Bedogni, S. Campanari, P. Iora, et al., J. Power Sources 171 (2007) 617–625.
[26] C. Qimei, Shanghai Jiaotong University doctor paper, Shanghai, 2007.
[27] H.L. Hao, H.S. Zhang, S.L. Weng, J. Power Sources 161 (2) (2006) 849–855.